JOURNAL OF MATERIALS SCIENCE 21 (1986) 3521–3527

# Diffuse phase transformations in neodymium-doped $BaTiO_3$ ceramics

P. MURUGARAJ, T. R. N. KUTTY
*Materials Research Laboratory, Indian Institute of Science, Bangalore 560012, India*
M. SUBBA RAO
*Department of Inorganic and Physical Chemistry, Indian Institute of Science, Bangalore 560012, India*

Phase transitions in $BaTiO_3$ doped with neodymium have been studied using temperature–capacitance measurements, differential scanning calorimetry, X-ray powder diffraction and electron paramagnetic resonance spectroscopy. The coexistence of a para-electric cubic phase with the ferroelectric tetragonal and orthorhombic phases is noticed within the temperature range corresponding to the stability region of the latter phases in undoped $BaTiO_3$. The broad maximum in the effective dielectric constant shifts to lower temperature with increase in neodymium content. The heat of transformation measured at the Curie point tends to zero above 3.5 at % Nd and the phase transition gradually approaches the second order. These are characteristics of a diffuse phase transformation. Using the quantitative results from the above studies, a $T$–$x$ topological diagram is constructed for the $BaTiO_3$–$x$Nd system where $x < 5.5$ at %. The phase contents vary with processing parameters as well as grain size, and the very existence of more than one phase in a given area of the $T$–$x$ diagram indicates the metastable thermodynamic equilibrium prevailing in $BaTiO_3$–Nd ceramics. The inhomogeneous distribution of lattice defects may be the major cause for such a behaviour.

## 1. Introduciton

$BaTiO_3$ ceramics doped with lower amounts of donor impurities (< 0.5 at %) are dark coloured and semiconducting even when they are sintered in air [1]. When cooled at definite rates (75 to 150 K $h^{-1}$) these ceramics show a positive temperature coefficient of resistance (PTCR) around the Curie temperature ($T_C$). If the cooling rate is slow (5 to 10 K $h^{-1}$) the same ceramics become insulating, with an effective dielectric constant $\varepsilon_{eff} > 10^5$ resulting in grain-boundary layer capacitance [1–4]. At donor levels greater than 0.5 at % and air as the sintering atmosphere, $BaTiO_3$ ceramics are light coloured and insulating, independent of cooling rate, with $\varepsilon_{eff}$ greater than those of conventional $BaTiO_3$ ceramics [2, 5]. The high $\varepsilon_{eff}$ in the above cases is due to their microstructure in which the grain-boundary layers are insulating and the grain interiors are semiconducting [6].

Temperature–capacitance curves indicate that $T_C$ shifts to lower temperatures with donor concentration [7, 8]. Electron paramagnetic resonance (EPR) showed that some fraction of the n-doped $BaTiO_3$ is cubic even at room temperature, and that the cubic fraction increases with donor content [9, 10]. The coexistence of more than one phase over a range of temperature is characteristic of a diffuse phase transformation (DPT) [11, 12]. The presence of a cubic phase has considerable importance with respect to the electrical properties of $BaTiO_3$ ceramics because the energy levels of the acceptor states are differently located in the cubic as compared to the tetragonal phase [9, 13]. Therefore the DPT behaviour of n-doped $BaTiO_3$ has practical significance in the production of ceramic capacitors.

Due to the DPT behaviour, the temperature–capacitance curves of n-doped $BaTiO_3$ show broad maxima and large deviations from the Curie–Weiss law. The nature of the DPT cannot be described by the classical theory of ferroelectric transitions. Its origin is not very clear and is said to be associated either with compositional or thermal fluctuations or with intergranular strains [14–17]. Point defects arising from inherent non-stoichiometry can also induce DPT behaviour [18]. A diffuse type of transition is noticed in a number of perovskite-type solid solutions such as $Ba(Ti_{1-y}Zr_y)O_3$ [19], $(Ba_{1-y}Sr_y)TiO_3$ [11], $Ba(Ti_{1-y}Sn_y)O_3$ [20] and $Ba(Nb_{1.5}Zr_{0.25})O_{5.25}$ [21]. A lowering of $T_C$ due to n-type impurities has been reported for $BaTiO_3$ by a number of previous workers. However, no reports exist on the DPT behaviour of $BaTiO_3$ ceramics doped with donor impurities [7, 8, 22].

## 2. Experimental procedure

$BaTiO_3$ with very low background impurities (Mn < 0.1, Fe < 1 $\mu$g $g^{-1}$) was prepared from the successive precipitation of the precursor oxalate, $BaTiO(C_2O_4)_2 \cdot 4H_2O$. $BaTiO_3$ doped with lanthanum or neodymium (0.05 to 5.5 at %) was prepared by co-precipitation in the precursor, and the resulting product was adjusted with $TiO_2$ such that the final composition is $(Ba_{1-x}La_x)TiO_{3+y}$ ($y \simeq x/2$). Doping with iron or manganese was carried out in solution

0022–2461/86 $03.00 + .12 

and the amounts incorporated in the precipitate (< 0.1 at %) were determined by atomic absorption spectrophotometry (Perkin-Elmer 2380) or quantitative EPR using MgO–Mn as the internal standard. Discs of 10 mm diameter and 1 mm thickness were sintered in air for 6 h at 1650 K and the samples were cooled slowly after sintering (10 to 20 K $h^{-1}$). The average grain size decreased from 25 $\mu$m for pure $BaTiO_3$ to $\leqslant 2\,\mu$m with donor content. With a slow heating rate under a lower partial pressure of oxygen than in air, grain growth could be achieved in ceramics with donor levels above 1 at %. The sinter densities were around 95 to 97%. The EPR spectra were recorded under conditions similar to those employed earlier [9], using a Varian E 109 X-band spectrometer in the range 80 to 523 K. The EPR intensity mentioned throughout this article is the double integrated intensity calculated from an empirical relation [23]

$$\mathrm{DII} = \frac{(\text{signal height})\,(\text{signal width})^2}{(\text{gain})\,(\text{sample weight})\,(\text{modulation amplitude})\,(\text{power})^{1/2}} \quad (1)$$

The X-ray investigations were carried out with a powder diffractometer (Philips PW-1050/76) using Cu$K\alpha$ radiation. The heat of transformation of the ferroelectric–para-electric phase change was measured with a Dupont differential scanning calorimeter (DSC) with high-purity $NH_4NO_3$ as the calibrant. For the electrical measurements, electroless nickel electrodes were deposited followed by nickel electroplating and annealing at 550 K. The effective dielectric constants were measured using a bridge having a seperate oscillator and detector. The temperature of the sample was slowly varied (1 K $min^{-1}$) from 150 to 450 K.

## 3. Results

### 3.1. Temperature–capacitance characteristics

Fig. 1 shows the temperature dependence of $\varepsilon_{eff}$ for $BaTiO_3$ ceramics with varying concentration of neodymium. $\varepsilon_{eff}$ values around $T_C$ are averages of those measured during heating or cooling cycles. For the undoped specimens the peaks in the $\varepsilon_{eff}$ curve coincide with the rhombohedral–orthorhombic $\sim 195$ K ($T_{R-O}$), orthorhombic–tetragonal $\sim 278$ K ($T_{O-T}$) and tetragonal–cubic $\sim 400$ K ($T_C$ or $T_{T-C}$) phase transitions. With neodymium content below 0.5 at %, the peak around 400 K broadens whereas those around 278 and 195 K are not observable, possibly because of the high $\varepsilon_{eff}$ associated with the grain-boundary layer capacitance. With further increase in donor concentration, the effective dielectric constant diminishes accompanied by a shift in $T_C$ to lower temperatures. The $T_{R-O}$ and $T_{O-T}$ values are slightly raised to higher temperatures. The capacitance peaks around these ferroelectric transitions are broad, so that clear distinction of the transition temperature becomes difficult.

### 3.2. Differential scanning calorimetry

The Curie point measured by DSC agreed fairly well with those determined by the capacitance measurements. The enthalpy of the tetragonal to cubic transformation ($\Delta H_{T-C}$) was determined for $BaTiO_3$ with various neodymium contents. As is evident from Fig. 2, these values decrease with neodymium concentration of the donor. DSC tracings are smeared out in samples containing Nd > 3 at %, so that the accuracy of the measurement is low. Under such conditions, the detection of the transformation temperature by DSC becomes difficult. The DSC results indicate that at higher donor concentrations the first-order transformation may be changing into a second-order transformation.

### 3.3. X-ray powder diffraction data

The sintered specimens were ground to a uniform powder of 200 mesh size for X-ray diffraction. The lattice parameters determined with silicon as the internal standard and using least square error analysis showed that $a_0$ increases from 0.3993 to 0.4007 nm; $c_0$ decreases from 0.4035 to 0.4006 ($\pm 0.0002$) nm at 300 K with the incorporation of 4 at % Nd, indicating that the sample containing 4 at % Nd is completely cubic at room temperature. Studies of the X-ray diffraction intensities of a number of reflections indicated the coexistence of more than one phase at room temperature for $BaTiO_3$ containing less than 4 at % Nd. The pairs of reflections considered are (2 0 0) and (0 0 2), (3 0 1) and (1 0 3) as well as (4 0 0) and (0 0 4). The relative variations of the integrated intensities of these pairs are measured to determine the phase content. For 100% tetragonal phase, the integrated intensity of (2 0 0) and (0 0 2) reflections are in the ratio 2 : 1. For 100% cubic phase, (0 0 2) is absent while the (2 0 0) reflection acquires a correspondingly

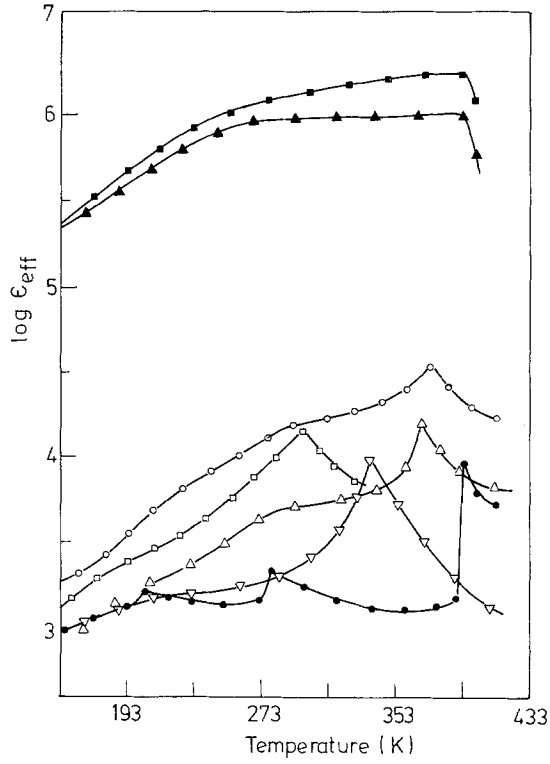


*Figure 1* Variation of effective dielectric constant at 1 kHz with temperature for $BaTiO_3$–$x$ at % Nd ceramics: $x$ = (●) 0, (■) 0.3, (▲) 0.5, (○) 1.0, (△) 1.2, (▽) 2.2, (□) 3.8%.

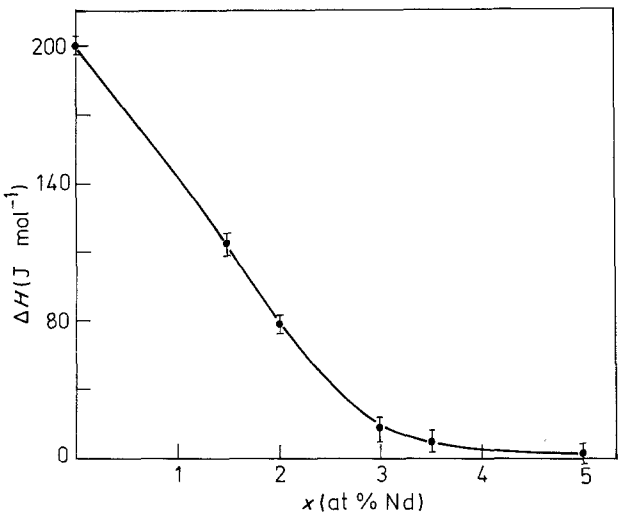


*Figure 2* Heats of transformation at ferroelectric to paraelectric phase transition determined by DSC for $BaTiO_3-x$ at % Nd ceramics.

higher intensity. Hence the intensity ratio $I_{(002)}/(I_{(200),(020)} + I_{(002)})$ approaches zero. In the case of a sample with mixed tetragonal and cubic phases, the intensity varies between 0.33 and zero.

Since the intensity ratio by the polymorphic method [24] may underestimate the cubic phase content, a calibration method similar to that of Tôraya *et al.* [25] is used to measure the intensity of these two reflections [26]. Samples for calibration were prepared by mixing various proportions of 100% tetragonal (undoped) $BaTiO_3$ and 100% cubic (doped) $BaTiO_3$. The maximum deviation from linearity is around 4%. With increase in neodymium content, the cubic fraction increases at room temperature. $BaTiO_3$–Nd is nearly completely cubic at 300 K when Nd $\geqslant$ 3.6 at % (Fig. 3). The ceramics with 1 at % Nd have $\sim$ 6.5% by weight of the cubic phase. The cubic phase content, as shown in Fig. 3, slightly increases with the duration of sintering at a given temperature. The other pairs of X-ray reflections such as (4 0 0) and (0 0 4) can be used for the phase content determinations. However, the intensity measurements of the back-reflections are partially affected by crystallographic textures possibly arising from the influence of varying internal stress in the microstructure. In this regard, we found that (2 0 0) and (0 0 2) reflections are better suited, and with the profile analysis technique an accuracy of $\pm$ 5 wt % in individual phases can be obtained.

## 3.4. EPR studies

In previous publications dealing with EPR studies on donor-doped $BaTiO_3$, [27–29] we have shown that the acceptor states are activated during the tetragonal-to-cubic phase transition and consequently trap electrons. The acceptor states arise from neutral barium vacancies and from background impurities such as manganese, iron etc. The EPR signal with $g = 1.997$, arising from singly ionized barium vacancies ($V'_{Ba}$), appears only in the cubic phase at donor concentration of less than 0.5 at %. The intensity of the $g = 1.997$ signal at 300 K increases with neodymium at high donor contents and has identical values at 300 and 400 K for $BaTiO_3$–4 at % Nd. This may be indicative of the existence of a cubic phase at room temperature.

For further verification, manganese in low concentration was used as a probe. With Mn $\sim$ 0.01 at % in $BaTiO_3$–0.2 at % Nd, no EPR signal due to manganese is observed in the tetragonal phase, whereas the signal arising from the $|+\frac{1}{2}m_I\rangle \leftrightarrow |-\frac{1}{2}m_I\rangle$ transition of $Mn^{2+}$ ($^6S_{5/2}$, $d^5$) appears above $T_C$. Keeping a constant manganese concentration (0.005 at %), $BaTiO_3$ ceramics of increasing neodymium contents were prepared. The variation in the intensities of $Mn^{2+}$ signals at different temperatures are plotted for these samples in Fig. 4. The temperatures at which the $Mn^{2+}$ signal acquires a high intensity corresponds to the Curie point of the bulk of the ceramics, which agrees with that obtained from the capacitance measurements. Fig. 4 shows that this temperature is lowered with increase in neodymium content. With 4 at % Nd, the $Mn^{2+}$ intensity at 300 K is the same as that at 400 K indicating that $T_C$ is shifted to less than the room temperature. The $Mn^{2+}$ EPR signal intensity above $T_C$ for Nd > 1.5 at % is lower than that of $BaTiO_3$–1 at % Nd. This is due to the stabilization of part of the manganese in a higher oxidation state (mostly +3) in these samples as discussed in a previous report [27].

$Mn^{2+}$ also appears in the low-temperature

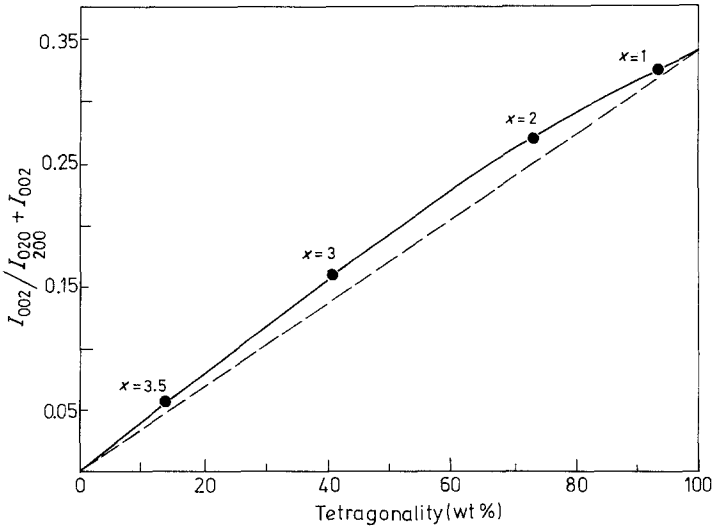


*Figure 3* Integrated intensity ratio of X-ray reflections against variation in phase composition. Dashed line is the ideal curve expected. Points are experimentally observed for $BaTiO_3-x$ at % Nd ceramics.

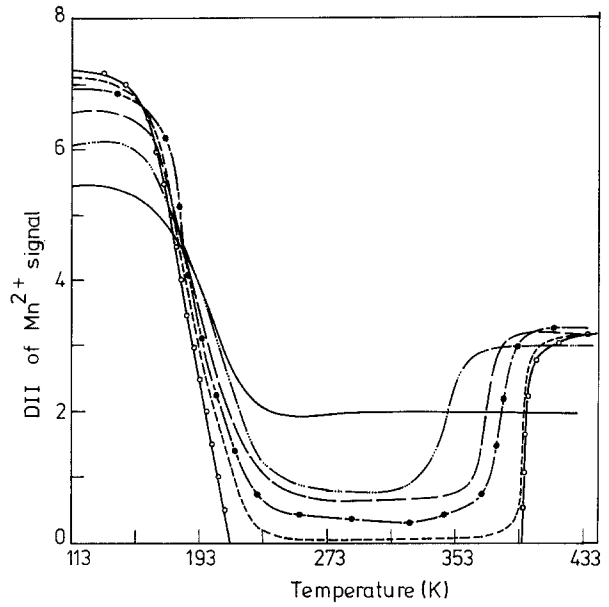


*Figure 4* Variation in double integrated intensity of $Mn^{2+}$ EPR signal with temperature for $BaTiO_3-x$ at % Nd ceramics: $x$ = (○) 0.2, (– – –) 0.5, (●) 1.0, (– –) 1.5, (– · –) 2.0, (——) 4.0%.

rhombohedral phase but not in the orthorhombic phase for $BaTiO_3$ with less than 0.5 at % Nd. It is evident from Fig. 4 that $T_{R-O}$ is only slightly shifted to a higher temperature with donor concentration. The persistence of the $Mn^{2+}$ signal in higher neodymium-containing samples above 240 K is indicative of the presence of a cubic phase along with the orthorhombic and tetragonal phases. The intensity (DII) of the $Mn^{2+}$ signal above the Curie point for $BaTiO_3$–2 at % Nd is 3.0. At 300 K the $Mn^{2+}$ intensity for the same specimen is 0.75. The intensity ratio 0.75/3.0 corresponds to 25% of cubic phase in this sample around room temperature. This value agrees with the X-ray intensity data shown in Fig. 3. A similar method has been extended to other specimens to determine the cubic phase content.

The EPR spectra of donor-doped $BaTiO_3$ containing 0.01 at % Fe are useful in monitoring the orthorhombic phase content. Earlier we have reported that $Fe^{3+}$ iron impurity located near an oxygen vacancy, the $Fe^{3+}-V_O$ defect complex, gives rise to two signals in the tetragonal phase with $g$ = 5.542 and 11.831 which are $g_\perp$ and $g_\parallel$ components of the $Fe^{3+}-V_O$ centre with axial symmetry [29]. In the orthorhombic phase the intensity of the $g$ = 11.831 signal remains the same but that of $g$ = 5.542 decreases. There appears a new signal with $g$ = 4.437 (Fig. 5). These three signals have been assigned to $g_x$, $g_y$ and $g_z$ components arising from an $Fe^{3+}-V_O$ centre in a rhombic field [29]. In both cubic and rhombohedral phases the $Fe^{3+}-V_O$ signals are absent. At constant iron concentration (0.01 at %), $BaTiO_3$ ceramics with increasing neodymium contents were prepared. The changes in the intensities of $Fe^{3+}-V_O$ signals at different donor concentrations are shown in Fig. 5a (300 K). The temperature variations of these signals for a given donor concentration are shown in Fig. 5b. The $g$ = 4.437 signal is indicative of the orthorhombic phase. The intensity ratio $I_{4.437}/I_{5.542}$ can be used to determine the orthorhombic phase content, which is found to be unity in the 100% orthorhombic phase of $BaTiO_3$ with less than 0.5 at % Nd over the appropriate temperature ranges.

### 3.5. The $T-x$ topological diagram

With the aid of the X-ray powder diffraciton and EPR data, the relative abundance of the phases could be determined at various temperatures for different concentrations of neodymium. Table I gives typical quantitative values of phase contents for $BaTiO_3-x$Nd ceramics at various temperatures and $x$ values. The topology of the $T-x$ diagram is shown in Fig. 6. The major phases are shown in capital letters, while the minor phases in decreasing order of abundance from left to right are given in small letters. The upper curve

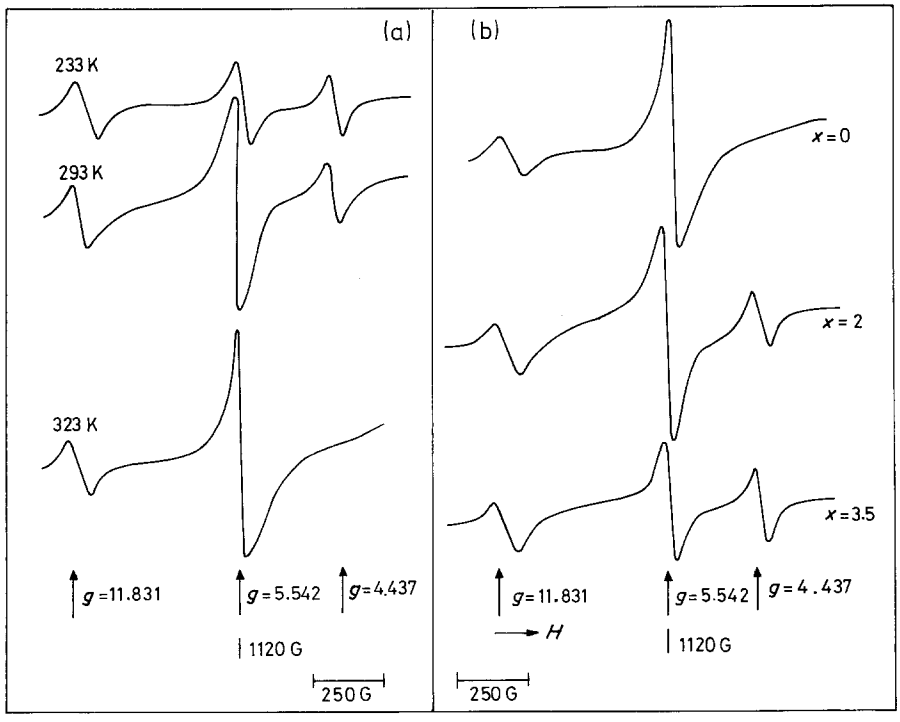


*Figure 5* EPR spectra of 0.01 at % Fe-doped $BaTiO_3-x$ at % Nd system: (a) variation of $Fe^{3+}-V_O$ signal in $BaTiO_3$–2 at % Nd ceramics with temperature, (b) variation of $Fe^{3+}-V_O$ signal at room temperature for $BaTiO_3-x$ at % Nd.

TABLE I Typical examples of relative phase contents (wt %) in $BaTiO_3$–$x$ at % Nd ceramics*

| Temperature (K) | $x$(at %)† | | | | | |
|---|---|---|---|---|---|---|
| | 0 | 0.5 | 1 | 2 | 3 | 4 |
| 400 | 100 (C) | 100 (C) | 100 (C) | 100 (C) | 100 (C) | 100 (C) |
| 380 | 100 (T) | 97 (T) | 92 (T) | 100 (C) | 100 (C) | 100 (C) |
| | | 3 (C) | 8 (C) | | | |
| 333 | 100 (T) | 97 (T) | 93 (T) | 75 (T) | 100 (C) | 100 (C) |
| | | 3 (C) | 7 (C) | 25 (C) | | |
| 273 | 100 (T) | 97 (T) | 94 (T) | 71 (T) | 40 (T) | 100 (C) |
| | | 3 (C) | 6 (C) | 25 (C) | 55 (C) | 2 (O) |
| | | | | 4 (O) | 5 (O) | |
| 263 | 100 (O) | 90 (O) | 90 (O) | 72 (O) | 45 (O) | 100 (C) |
| | | 7 (T) | 4 (T) | 3 (T) | 55 (C) | 2 (O) |
| | | 3 (C) | 6 (C) | 25 (C) | | |

*The processing parameters were kept constant for all the test samples. Heating rate = 5 K $min^{-1}$; sintering temperature = 1650 K; sintering time: 6 h; cooling rate: 10 to 20 K $h^{-1}$.
†C = cubic, T = tetragonal, O = orthorhombic.

represents the transition from para-electric to ferroelectric phase, while the lower lines demarcate the areas in which one of the ferroelectric phases has the highest abundance. There is extensive coexistence of two or more phases in the tetragonal and orthorhombic regions, while rhombohedral and cubic phase regions do not show such coexistence.

Fig. 6 also shows that the Curie point is shifted to a lower temperature, but the other two transition temperatures are slightly increased with increase in donor concentration. The transformation characteristics of $BaTiO_3$ with less than 0.5 at % Nd are nearly the same as that of undoped $BaTiO_3$. The right-hand side of the diagram shows that the para-electric cubic phase directly transforms to the ferroelectric rhombohedral phase. In the intermediate compositions, the stability regions of the orthorhombic and tetragonal phases become narrower with increasing neodymium content and they continue to coexist with the cubic phase until about 5.3 at % Nd. The quantitativeness of Fig. 6 is found to be dependent on processing parameters such as the method of donor doping, the sintering schedule and also on the average grain size of the ceramic. In the grain-grown specimen, the relative concentration of the para-electric cubic phase is lower than the normally sintered sample of the same composition. This is seen from the lowering of the room-temperature intensities of the $Mn^{2+}$ signal (Fig. 7a) and the $V_{Ba}$ signal (Fig. 7b) with increase in grain size for a constant dopant concentration. However, the general features of Fig. 6 remain unaltered.

## 4. Discussion

The coexistence of two or more phases within a range of temperature and possibly composition is characteristic of DPT behaviour. Such a coexistence of phases is known in $BaTiO_3$ solid solutions formed by isovalent ionic substituents such as $(Ba_{1-y}Sr_y)TiO_3$ (A-site substituents) [11] and $Ba(Ti_{1-y}Zr_y)O_3$ (B-site substituents) [19]. In both cases the Curie points are lowered with increase in $y$ value. In the case of $(Ba_{1-y}Sr_y)TiO_3$, $T_{T-O}$ and $T_{O-R}$ are lowered with $y$ value whereas for $Ba(Ti_{1-y}Zr_y)O_3$, the corresponding temperatures are raised. For neodymium-doped

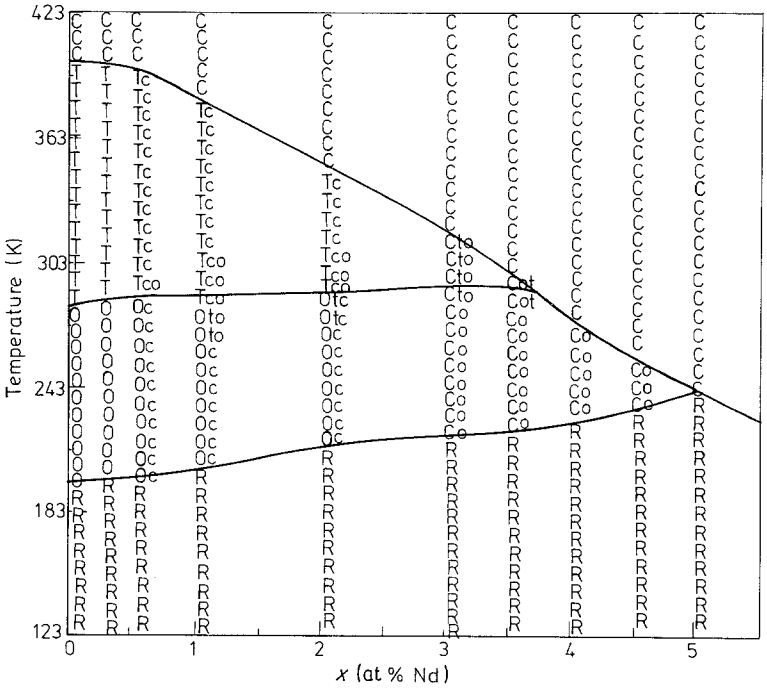


*Figure 6* $T$–$x$ topological diagram for $BaTiO_3$–$x$ at % Nd ceramics. Major phases are shown in capital letters while the minor phases in decreasing order of abundance from left to right are given in small letters. (C = cubic, T = tetragonal, O = orthorhombic, R = rhombohedral).

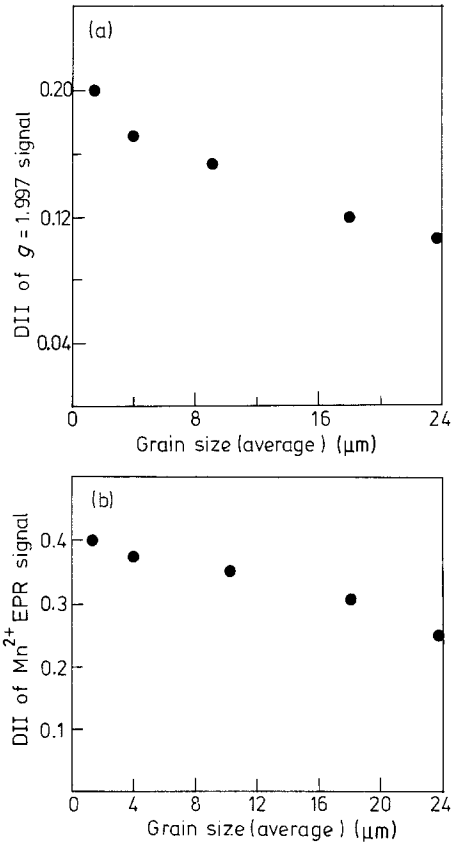


*Figure 7* Variation in double integrated intensity of (a) $g = 1.997$ signal at room temperature and (b) $Mn^{2+}$ signal at 298 K with average grain size for grain-grown $BaTiO_3$–1.0 at % Nd ceramics.

$BaTiO_3$, the $T_C$ value is lowered while T–O and O–R transition temperatures are marginally raised. In this regard neodymium-doped $BaTiO_3$ differs from the behaviour of solid solutions with A- and B-site isovalent substituents.

The $T$–$x$ diagram shown in Fig. 6 also differs in several aspects from those of the isovalent-ion substituted solid solutions. For $(Ba_{1-y}Sr_y)TiO_3$, the coexistence region is between the ferroelectric and para-electric limit curves, bordering the single-phase regions in the phase diagrams [11]. In Fig. 6, the coexistence is not limited to the boundaries but throughout what ought to have been the single-phase regions of the tetragonal and orthorhombic phases. Another distinguishing feature is that the amount of cubic phase coexisting with the ferroelectric phases (tetragonal and orthorhombic) does not continuously vary with temperature except at a given point which is the effective Curie temperature for the bulk of the sample. In the $Ba(Ti_{1-y}Zr_y)O_3$ system, the coexistence of tetragonal and orthorhombic phases with the cubic phase is restricted to a narrow temperature region, for a given composition. The third distinguishing feature of the $BaTiO_3$–Nd system is that the percentage of cubic phase stabilized within the tetragonal and orthorhombic phase regions varies with the processing parameters at a constant donor concentration. For these reasons, the mechanism of the origin of the DPT in isovalent-ion substituted solid solutions may be different from those of aliovalent-ion substituted materials.

In the case of isovalent-ion substituted solid solutions, the DPT is assumed to be due to polarized microregions (Känzig regions) with different Curie temperatures; differences in $T_C$ arise from the mechanical stress distribution or due to a variation in chemical composition. Implied in this concept is the increased stress in the microstructure during the cubic-to-tetragonal transition which is largely compensated by ferroelectric domains. For ceramics of smaller grain size (a few micrometres), this compensation is incomplete and is said to be the major reason for the observed distribution of Curie temperatures. The contribution from chemical inhomogeneity (resulting from the Ti/Zr ratio) to the distribution of $T_C$ is said to be small. For $(Ba_{1-y}Sr_y)TiO_3$, the DPT behaviour has been explained in terms of the coexistence of two phases in thermal equilibrium [11].

In the case of aliovalent-impurity substituted solid solutions, the formation of lattice defects additionally influences the transformation behaviour. For donor-type impurities in $BaTiO_3$, compensation is through conduction electrons as well as through cation vacancies [4]. The electron compensation may either increase the number of conduction electrons or may change the oxidation state of lattice constituents, most likely $Ti^{4+}$ to $Ti^{3+}$. Of the different possibilities, the vacancies at the A cation sites are more energetically favourable than at the B-site. It is reported that aliovalent substituents and cationic vacancies are not uniformly distributed throughout the $BaTiO_3$ ceramics [22]. TEM studies on $BaTiO_3$ ceramics with different aliovalent additives have shown that microstructural inhomogeneity leads to the grain core–grain shell relation [22, 30]. The chemical inhomogeneity arises during the process of reactive sintering. A heterogeneous defect distribution in donor-doped $BaTiO_3$ ceramics is also reported in the literature wherein the grain-boundary layer has a higher $V_{Ba}$ concentration and nearly complete vacancy compensation, whereas a mixed compensation prevails within the bulk of the grains [4].

Any perturbation within the $BaTiO_3$ lattice shifts the Curie point. This can be due to iso- or aliovalent substituents, lattice defects such as anion or cation vacancies or even conduction electrons [31]. When such defects are inhomogeneously distributed, there will be a spread of $T_C$ values. This is all the more obvious from the decrease in the heats of transformation with increased $x$ value. Since the enthalpy change tends to zero (Fig. 2), the free-energy change around $T_C$ should also be very small. This means that the free energy of different phases have nearly the same value, and therefore extensive coexistence of different phases is possible. Slight changes of the chemical potential can cause noticeable changes in the Curie point and also the phase contents. This is evident from the features of the $T$–$x$ diagram (Fig. 6). According to the Gibbs phase rule for binary systems, a maximum of three phases can coexist only at an invariant point. In Fig. 6, three phases are coexisting in a given area of the diagram. This apparent contradiction of the phase rule indicates that Fig. 6 does not represent an equilibrium state. It can be better treated as a metastable equilibrium situation frozen in

from the high-temperature sintering conditions. It is obvious, therefore, that the sintering parameters will alter the phase content.

Kell and Helicar [32] considered that the high and broad $\varepsilon_{eff}$ curves around $T_C$ are due to the coexistence of more than one ferroelectric phase. In ceramic capacitors such coexistence may be due to the semicontrolled, inhomogeneous distribution of substituents as well as the lattice defects (mostly cationic vacancies in the present case). The same situation cannot be prevailing in single crystals. Preparation of $BaTiO_3$ single crystals with more than 1 at % Nd is found to be difficult, both by flame fusion and the flux method, and therefore no comparison with the single crystal samples could be carried out.

## References


1. O. SABURI, *J. Phys. Soc. Jpn* **14** (1959) 1159.
2. W. HEYWANG, *J. Mater. Sci.* **6** (1971) 1214.
3. H. BRAUER, *Z. Angew. Phys.* **29** (1970) 282.
4. J. DANIELS and R. WERNICKE, *Philips Res. Repts* **31** (1976) 544.
5. G. H. JONKER, *Solid State Electron.* **7** (1964) 895.
6. K. S. MAZDIYASNI, *Bull. Amer. Ceram. Soc.* **63** (1984) 591.
7. M. KHAN, *J. Amer. Ceram. Soc.* **54** (1971) 455.
8. E. C. SUBBARAO and G. SHIRANE, *ibid.* **42** (1959) 279.
9. T. R. N. KUTTY, P. MURUGARAJ and N. S. GAJBHIYE, *Mater. Res. Bull.* **20** (1985) 565.
10. P. MURUGARAJ and T. R. N. KUTTY, *ibid.* **20** (1985) 1473.
11. D. BARB, E. BARBULESCU and A. BARBULESCU, *Phys. Status Solidi* **74a** (1982) 79.
12. G. A. SMOLENSKII, *J. Phys. Soc. Jpn* **28** suppl. (1970) 26.
13. T. R. N. KUTTY and L. GOMATHI DEVI, *Mater. Res. Bull.* **20** (1985) 793.
14. V. I. FRITSBERG, in Proceedings of International Meeting of Ferroelectricity Prague, June/July 1966, Vol. 1 (Czech Academy of Sciences, 1966) p. 163.
15. V. I. FRITSBERG, A. J. BOCK and K. J. BORMAN, *Ferroelectrics* **8** (1975) 495.
16. A. J. BURGGRAAF and K. KEIZER, *Mater. Res. Bull.* **10** (1975) 521.
17. H. T. MARTIRENA and J. C. BURFOOT, *J. Phys. C* **7** (1974) 3182.
18. S. SHIRASAKI, K. THAKAHASHI and K. KAKEGAWA, *J. Amer. Ceram. Soc.* **56** (1973) 430.
19. D. HENNINGS, A. SCHNELL and G. SIMON, *ibid.* **65** (1982) 539.
20. T. N. VERBITSKAYA, YU. M. POLAVKO and B. YA. YAZYTSKII, *Sov. Phys. Solid State* **9** (1968) 2634.
21. G. GOODMAN, *J. Amer. Ceram. Soc.* **43** (1960) 105.
22. D. HENNINGS and G. ROSENSTEIN, *ibid.* **67** (1984) 249.
23. S. S. EATON and G. R. EATON, *Bull. Magn. Resonance* **1** (1979) 130.
24. H. P. KLUG and L. E. ALEXANDER, "X-ray diffraction procedures" (Wiley, New York, 1974) p. 531.
25. H. TÔRAYA, M. YOSHIMURA and S. SŌMIYA, *J. Amer. Ceram. Soc.* **67** (1984) C119.
26. W. PARRISH, T. C. HUANG and G. L. AYERS, *Trans. Amer. Crystallogr. Assoc.* **12** (1976) 55.
27. T. R. N. KUTTY, P. MURAGARAJ and N. S. GAJBHIYE, *Mater. Lett.* **2** (1984) 396.
28. T. R. N. KUTTY and P. MURUGARAJ, *ibid.* **3** (1985) 195.
29. P. MURUGARAJ and T. R. N. KUTTY, *J. Mater. Sci. Lett.* **5** (1986) 171.
30. B. S. RAWAL, M. KAHN and W. BUESSEM, in "Advances in Ceramics", Vol. 1, edited by L. M. Levinson (American Ceramic Society, Columbus, Ohio, 1981) p. 172.
31. K. H. HÄRDTL and R. WERNICKE, *Solid State Electron.* **10** (1972) 153.
32. R. C. KELL and N. J. HELICAR, *Acoustica* **6** (1956) 235.



*Received 21 October*
*and accepted 18 December 1985*